Gao *et al.*
European Journal of Medical Research (2024) 29:541
https://doi.org/10.1186/s40001-024-02146-2

European Journal of Medical Research

RESEARCH

Open Access

The role of CISD1 reduction in macrophages in promoting COPD development through M1 polarization and mitochondrial dysfunction

Jiameng Gao[1,2†], Meiyuan Dong[1†], Weibin Tian[1†], Junyi Xia[1], Yuhao Qian[2], Zhilong Jiang[2], Zhihong Chen[2*] and Yao Shen[1*]

Abstract

Background The mitochondrial dysfunction and oxidative stress imbalance caused by macrophage polarization play a role in the progression of COPD, with CDGSH iron–sulfur domain-containing protein 1 (CISD1) playing a key role. This study revealed the role and mechanism of CISD1 in smoke-induced macrophages.

Methods Using a pure cigarette smoke exposure-induced COPD mouse model, stimulation of Raw264.7 macrophages with cigarette smoke extract mimics the COPD environment. Knocking down CISD1 expression in macrophages and combining it with high-throughput sequencing to obtain subsequent differentially expressed genes and pathways. Macrophage polarization tendency under different treatments was determined using flow cytometry. Meanwhile, Mitosox, JC-1, DCFH-DA fluorescence intensity was measured to detect mitochondrial function and cellular oxidative stress levels. Western Blot technique was employed to validate autophagy (mitochondrial autophagy) pathway-related proteins. In addition, Elisa technique was used to measure inflammatory factors (IL-6, TNF-a) in the cell supernatant after co-culturing macrophages (Raw264.7) with epithelial cells (MLE12).

Results CISD1 is underexpressed in peripheral blood monocytes of COPD patients. Under in vitro conditions, we verified that cigarette smoke (smoke extract) indeed inhibits CISD1 expression in macrophages. Subsequently, we found that macrophages with knocked-down CISD1 tend to polarize towards M1 phenotype, and exhibit signs of mitochondrial dysfunction and oxidative stress imbalance. In addition, we observed significant activation of the autophagy pathway in CISD1-inhibited macrophages, with upregulation of LC3A/B and downregulation of p62 protein, as well as increased expression of mitochondrial autophagy-related proteins (PINK1, PARKN). Furthermore, co-culturing CISD1-knockdown macrophages (Raw264.7) with epithelial cells (MLE12) resulted in upregulation of inflammatory factors in the supernatant.

Conclusions Smoke-induced reduction of CISD1 in macrophages promotes M1 polarization and mitochondrial dysfunction by activating the autophagy pathway, thereby promoting the occurrence and development of COPD.

Keywords Chronic obstructive pulmonary disease (COPD), CDGSH iron–sulfur domain-containing protein 1 (CISD1), Autophagy, Mitochondrial dysfunction, Microphage

[†]Jiameng Gao, Meiyuan Dong and Weibin Tian are equally contributed to this work

*Correspondence:
Zhihong Chen
chen.zhihong@zs-hospital.sh.cn
Yao Shen
shenyao1976@126.com

Introduction

Chronic Obstructive Pulmonary Disease (COPD) is a common, preventable, and treatable disease characterized by persistent airflow limitation [1]. Its pathological hallmarks include chronic bronchitis and/or emphysema, and its etiology is linked to multiple factors such as smoking, air pollution, occupational dust, imbalance of proteases and antiproteases, and infections. The disease has a complex pathogenesis, with frequent exacerbations that often result in a poor prognosis [2].

Recent literature suggests that the polarization of lung macrophages plays a crucial role in COPD pathogenesis, especially the impact of mitochondrial dysfunction on macrophage polarization, which may be a key mechanism underlying COPD progression [3]. Mitochondrial dysfunction encompasses various pathological changes, including imbalances in mitochondrial fusion and fission, impaired autophagy, abnormal accumulation of mitochondrial reactive oxygen species (ROS), and disruption of mitochondrial membrane potential (MMP) [4, 5]. Among these, impaired mitochondrial autophagy significantly affects mitochondrial function and exacerbates the dysfunction phenotype [6]. Mitochondrial autophagy, a specialized form of autophagy, involves multiple mechanistic pathways. When mitophagy is impaired, cellular vitality declines, leading to organelle damage and impaired cellular function [7].

CDGSH iron–sulfur domain-containing protein 1 (CISD1), also known as mitoNEET, is an iron-containing protein localized on the outer mitochondrial membrane [8]. As a member of the NEET protein family, CISD1 is involved in various cellular processes, particularly in maintaining redox balance (cellular ROS homeostasis), regulating iron metabolism, and supporting mitochondrial function [9]. Recent research has explored the role of CISD1 in cardiovascular diseases [10], cancer [11], and neurodegenerative disorders. However, its role in COPD, particularly in COPD-related macrophages, remains poorly understood. This study aims to investigate the role of CISD1 in smoke-induced macrophage polarization, with a focus on the involvement of autophagic mechanisms, and to elucidate the subsequent impact on epithelial cells, specifically the production of inflammatory mediators.

Materials and methods

Bioinformatic analyses

In this study, we employed bioinformatics analysis using data from the publicly available Gene Expression Omnibus (GEO) database. Specifically, we retrieved the dataset GSE146560 [12], which contains transcriptomic data of peripheral blood mononuclear cells (PBMCs) from smokers (n = 12) and healthy controls (n = 4). The data were accessed through the GEO platform (https://www.ncbi.nlm.nih.gov/geo/). The expression levels of CISD1 were analyzed to identify differential transcriptional profiles between the two groups. We used standard preprocessing steps, including normalization and background correction, to ensure data quality. Following this, we applied statistical analysis to assess the differential expression of CISD1 between smokers and healthy individuals. Statistical significance was determined using a threshold of $p < 0.05$.

This dataset was downloaded from the GEO database in MINiML format, which includes complete platform, sample, and series records. For datasets that were not normalized, log2 transformation was applied. In addition, we utilized the normalize.quantiles function from the preprocessCore package in R for normalization. Based on platform annotation, probe IDs were converted to gene symbols, and probes corresponding to multiple genes were excluded. For probes corresponding to the same gene, an average value was calculated. In cases of batch effects within the same dataset or platform, we employed the removeBatchEffect function from the limma package in R to remove these effects.

For multi-dataset or multi-platform analyses, we extracted common gene symbols across datasets, marked different datasets or platforms as separate batches, and again used the removeBatchEffect function to eliminate batch effects. We evaluated the success of the normalization process using box plots, and assessed batch effects by comparing principal component analysis (PCA) plots before and after batch correction [13–15].

Cell culture and regents

The Raw264.7 and MLE12 cell lines used in this study were obtained from the Chinese Academy of Sciences. Raw264.7 and MLE12 cells were cultured at 37 °C in a 5% CO2 humidified atmosphere using DMEM medium (Servicebio, G4511, China) supplemented with 10% FBS (BIOAGRIO, S1001-500, South America). 3-Methyladenine (3-MA, Selleck, Cat.S2767) was dissolved in heated sterile double distilled water to make a 200 mM stock solution and then added to the medium for a final concentration of 5 mM.

Preparation of cigarette smoke extract (CSE)

The aim of this study was to simulate the microenvironment of cigarette smoke exposure in cell culture. The choice of a 2% cigarette smoke extract (CSE) concentration is typically based on previous studies that have identified it as a biologically relevant concentration for in vitro experimentation [12]. This concentration of CSE also triggered inflammatory responses by upregulating cytokines like TNF-α, IL-1β, and IL-6, alongside

oxidative stress markers [16], and it doesn't cause excessive toxicity or cell death. The CSE solution was prepared freshly on the day of the experiment. The specific procedure was as follows: first, commercial cigarettes (each containing 2.5 mg of nicotine and 12 mg of tar, purchased from Shanghai, China) were drawn into a flask containing 10 mL of DMEM at a rate of one cigarette every 3 min using a vacuum pump. The pH of the CSE solution was adjusted to 7.4, and the OD (A320–A540) was maintained between 0.9 and 1.2. The CSE solution was then filtered through a 0.22 μm filter to remove bacteria and other microorganisms. This solution was considered as 100% CSE and was further diluted with DMEM medium to a working concentration of 2% for subsequent experiments, which were performed within 1 h of preparation as needed [16–19].

siRNA interference

siRNA specifically designed to target Raw264.7 was purchased from Sangon Biotech, Shanghai.

The design should follow these key principles: first, select a specific siRNA sequence that targets the gene of interest, ensuring its specificity. The sequence length should generally range between 19 and 25 nucleotides, as sequences longer than 30 nucleotides are prone to non-specific binding to other mRNAs. Second, utilize bioinformatics tools to design the siRNA sequence, and perform BLAST searches to avoid off-target effects, ensuring that the chosen sequence does not closely resemble non-target genes. The GC content should be maintained between 35 and 55% to optimize gene silencing efficiency. In addition, the siRNA target sequence is typically located within the coding sequence (CDS) of the target gene.

In this study, the working concentration of sirna was set at 50 nM and the transfection time was 24 h. After transfection, Western blot was performed for protein quantification, and siRNA-2 showed the best interference efficiency. Lipofectamine 8000 (Beyotime, C0533) was mixed with Opti-MEM and incubated at room temperature for 20 min before being added to Raw264.7 macrophages. After 24 h, intervention was initiated.

The sequence was sense (5'–3') UUCGGGUUGUCU UUCUGGAUCTT. Anti-sense (3'–5') UUCGGGUUG UCUUUCUGGAUCTT.

Animal model

Six-week-old male C57BL/6 mice were purchased from Beijing Vital River Laboratory Animal Technology Co., Ltd. and housed in the experimental animal center of Pudong Hospital affiliated to Fudan University. All animal experiments were conducted according to the protocol approved by the Animal Care and Use Committee of Pudong Hospital affiliated to Fudan University (SKWXZ-01). Mice were pair-fed. First, a CS exposure mouse model was established. The whole-body smoke exposure system consisted of an automatic smoke generator equipped with a programmable pump (#C-260, Shanghai Yuyan Scientific Instruments Co., Ltd.), an exposure chamber, and a laminar flow biological safety cabinet. To prevent exposure of the operators to second hand smoke, the exposure chamber was used inside the laminar flow biological safety cabinet. CS was generated by the automatic cigarette smoke generator and pumped into the exposure chamber. Mice (n = 5) were exposed to morning and evening, 6 days a week, for 3 months. The control group (n = 5) was kept in the same environment, including the same amount of food, without CS exposure. The control group (5 mice) was kept in the same environment, including the same amount of food, but was not exposed to CS. At the beginning of the fumigation, the model mice were fumigated with CS, and the control mice were exposed to another hut filled with normal air, and the operation was the same, except that they did not receive CS fumigation. At the end of the fumigation, all mice were released back to the central air supply in the Animal Experimentation Centre. Lung and bronchoalveolar lavage fluid (BALF) were collected from mice for H&E staining, immunohistochemistry (IHC), and measurement of inflammatory mediators.

Western blotting

Raw264.7 cells were collected by scraping after incubation in DMEM medium with corresponding treatments for the appropriate duration. The collected cells were lysed on ice in RIPA buffer containing 1% protease inhibitor. Protein extracts were obtained by high-speed centrifugation at 4 °C, 12000 rpm. Protein concentration was quantified using the BCA protein quantification kit (Thermo Fisher, Waltham, USA). Equivalent amounts of proteins were separated by SDS–PAGE gel electrophoresis, transferred onto PVDF membranes, blocked, and incubated overnight at 4 °C with primary antibodies. After washing with TBST (TBS containing 1% Tween), membranes were incubated with secondary antibodies for 60 min and protein levels were observed using the ECL protein blotting detection kit. Primary antibodies used were: CISD1 (Cat No. 16006-1-AP, Proteintech, USA, 1:10000), LC3A/B (Cat No. 4108S, Cell Signaling Technology, USA, 1:1000), SQSTM1/p62 (Cat No. 39749S, Cell Signaling Technology, USA, 1:1000), PINK1 (Cat No. 23274-1-AP, Proteintech, USA, 1:1000), Parkin (Cat No. 14060-1-AP, Proteintech, USA, 1:3000), β-actin (Cat No. 20536-1-AP, Proteintech, USA, 1:10000), GAPDH (Cat No. 60004-1-Ig,

Proteintech, USA, 1:10000)); secondary antibody: Peroxidase AffiniPure Goat Anti-Rabbit IgG (H + L) (Cat No. 33101ES60, Yeasen, China, 1:10000)).

The ChemiDocTM MP imaging system (BIO-RAD) evaluated these bands and quantified them using the ImageJ software (version 1.53v).All target protein was had been normalized using GAPDH or β-actin. Then each treatment group was compared with the control group, the target protein in the control group was considered as the baseline (value = 1), and the fold change value of the other group/control group was shown in the graph.

Immunohistochemistry

Lung tissues from control and smoke-exposed mice were embedded in paraffin and used for IHC analysis. Samples were stained with anti-F4/80 antibody (70076; CST, USA, 1:1000), CISD1 antibody (16006-1-AP; Proteintech, USA, 1:500), followed by incubation with HRP-conjugated anti-IgG antibody (ab205718; Abcam, UK, 1:400) and Donkey anti-Rabbit IgG (H + L) Highly Cross-Adsorbed Secondary Antibody, Alexa Fluor™ 594 (A21207, ThermoFisher, Waltham, MA, USA, 2.0 mg/mL) using standard protocols. Specific steps included: baking the slides in a constant temperature oven at 65 °C for 45 min; dewaxing in xylene I, II, III for 10 min each; antigen retrieval in sodium citrate buffer for 15 min, followed by PBS washes and blocking with 3% H2O2. Then, incubation with primary antibody overnight at 4 °C, followed by secondary antibody incubation, and DAB staining. Counterstaining with hematoxylin, dehydration, and mounting. Images were captured and analyzed using a microscope, with macrophage nuclei appearing green and CISD1 positive staining appearing purplish red.

HE staining

First, sequentially place the paraffin sections in environmentally friendly dewaxing solutions I and II, each for 20 min. Then, immerse them separately in anhydrous ethanol I and II for 5 min, followed by a 5-min immersion in 75% ethanol. Rinse with water. Next, soak the sections in hematoxylin staining solution for 3–5 min, followed by rinsing with tap water. Perform identification using identification solution, rinse with tap water, stain with a blue reagent, and rinse under tap water. Then, sequentially immerse the sections in 85% and 95% gradient ethanol for 5 min each for dehydration, followed by staining with eosin solution for 5 min. Finally, place the sections in anhydrous ethanol I, II, III for 5 min each, then clear with xylene I and II for 5 min each. Mount using a neutral mounting medium. Finally, examine the sections under a microscope and capture images for analysis.

ELISA

IL-6, TNF-α, and IL-1β levels were measured using commercially available enzyme immunoassay/ELISA kits (Biotechwell, Shanghai), according to the manufacturer's instructions. The detection limits for these assays were 15.6 ng/ml.

Measurement of intracellular and mitochondrial ROS levels and ROS levels in cells

According to the instructions, use the Reactive Oxygen Species Assay Kit (50101ES01, Yeasen, China) and MitoSOX Red Mitochondrial Superoxide Indicator (40778ES50, Yeasen, China). Resuspend cells in 100 μl of binding buffer and incubate protected from light for 30 min. Record the fluorescence of DCFH-DA (ROS) or Mitosox (mtROS) using flow cytometry to assess in different groups.

Measurement of JC-1

Using the JC-1 mitochondrial membrane potential fluorescent probe (40752ES60, Yeasen, China), according to the instructions, cells were resuspended in 100 μl of binding buffer and incubated in the dark for 30 min. Different groups of JC-1 conditions were recorded using flow cytometry.

Detection of CISD1 expression in monocytes from mouse lung tissue using flow cytometry

Briefly, lung tissues (40 mg/each mouse) from model and control group mice were digested with Collagenase IV (Sigma, C5138-100MG), which was diluted to a working concentration of 2 mg/mL, with 500 μL of solution used per mouse. The digestion was carried out at 37 °C for 2 h to prepare a single-cell suspension. Following red blood cell lysis, the cells were stained with flow cytometry antibodies and then analyzed on the machine. The fluorescent channels and corresponding antibodies used were:APC-Cyanine7: Zombie NIR™Fixable Viability Kit (Biolegend, Cat. 423105); PE-Cyanine7: anti-mouse/human CD11b (Biolegend, Cat. 101205); Qdot605: Brilliant Violet 605™ anti-mouse F4/80 Antibody (Biolegend, Cat. 123133); CoraLite® Plus 488: CISD1 Polyclonal antibody conjugated with CoraLite® Plus 488 (Proteintech, Cat. CL488-16006). The concentrations of the antibodies were used as recommended by the respective manufacturers.

Detection of M1/M2 polarization tendency in macrophages using flow cytometry

Raw264.7 cells were treated as required by the experiment, followed by flow cytometry antibody staining and subsequent analysis on the machine. The fluorescent

channels and corresponding antibodies used were: Parcific Blue: Brilliant Violet 421™ anti-mouse CD206 (MMR) (Biolegend, Cat. 141717); PE: Anti-mouse CD86 (Biolegend, Cat. 105007). The antibody concentrations were used according to the manufacturer's recommendations.

Co-culture system parameters

RAW264.7 macrophages and MLE-12 mouse lung epithelial cells were co-cultured, with MLE-12 cells seeded in the lower layer of a six-well plate and RAW264.7 cells seeded in the upper Transwell insert, allowing indirect interaction through soluble factors. The seeding densities were 500,000 MLE-12 cells per well in the lower layer and 100,000 RAW264.7 cells per well in the upper insert. Both cell types were cultured in DMEM supplemented with 10% FBS, penicillin, and streptomycin. After 24 h of co-culture, the supernatant was collected for the detection of inflammatory cytokines using ELISA.

Statistical analysis

All experiments were conducted at least three times independently. Data were shown as mean value ± SD. The statistical analyses were conducted using GraphPad Prism 8.4.2. The comparison between different experimental groups was analyzed by student *t* test and ANOVA. The overall survival rate was calculated using the Kaplan–Meier method and Cox's proportional hazards regression model. The log-rank test was used to calculate the statistical difference between groups. $P < 0.05$ was considered statistically significant.

Results

Smoke exposure leads to a decrease in CISD1 expression in monocyte-derived macrophages

To evaluate the clinical relevance of this study, we conducted a differential expression analysis of the CISD1 gene in peripheral blood monocytes from both healthy individuals and smokers using multiple datasets. As shown in Fig. 1A, CISD1 expression was reduced in smokers compared to healthy controls. In addition, CISD1 expression was found to be associated with biological processes such as neutrophil degranulation, neutrophil activation in immune responses, and pattern specification (Supplementary Fig. 1).

As depicted in Fig. 1B, we constructed a COPD mouse model by exposing mice to smoke for 3 months. The model was validated by examining lung tissue histopathology using HE staining, which confirmed the presence of COPD-like pathology (Fig. 1F). We also observed elevated levels of inflammatory factors, including TNF-α and IL-6, in bronchoalveolar lavage fluid (BALF) (Fig. 1C). Compared to the control group, mice in the smoke-exposed group exhibited macrophage aggregation in the lung bronchi and bronchial lumens (Fig. 1E). Immunohistochemical fluorescence co-localization showed reduced CISD1 expression in macrophages of smoke-exposed mice compared to controls (Fig. 1G). Flow cytometry of lung tissue from COPD and control mice further confirmed decreased CISD1 expression in macrophages (Fig. 1H).

Finally, we conducted in vitro validation by stimulating Raw264.7 macrophages with 2% cigarette smoke extract (2% CSE) for 24 h. Western blot analysis showed a decrease in CISD1 protein levels in macrophages following CSE stimulation (Fig. 1I).

Inhibiting CISD1 expression promotes macrophage polarization towards the M1 phenotype and inhibits M2 phenotype polarization

We transfected macrophages with small interfering RNA targeting CISD1 (si-CISD1), and after 24 h, we measured CISD1 protein levels using Western blotting. Compared to si-NC, the transfection efficiency of si-CISD1-1 was approximately 30%, while that of si-CISD1-2 was higher, around 60%. Therefore, we selected si-CISD1-2 for further experiments (Fig. 2A). Twenty-four hours after transfection with the selected si-CISD1, macrophages polarized towards the M1 phenotype with proportions of 15.2% and 42%, while M2 phenotype polarization decreased to 5.67% and 0.19%, respectively. Both M1 and M2 phenotype polarizations showed significant differences (Fig. 2B). In addition, we observed that after treating Raw264.7 cells with 2% cigarette smoke extract (2%CSE) for 24 h, compared to the NC group, macrophages polarized towards the M1 phenotype with proportions of 13.6% and 48.5%, while M2 phenotype polarization decreased to 9.87% and 1.26%, respectively. Both M1 and M2 phenotype polarizations exhibited statistical differences (Fig. 2C). ELISA analysis of TNF-α and IL-6 levels in the supernatant of macrophages after si-CISD1 transfection showed differences between the si-NC and si-CISD1 groups (Fig. 2D).

Furthermore, we investigated the mitochondrial ROS (MitoSOX), macrophage ROS (DCF) and membrane potential (JC-1) of Raw cells after si-CISD1 transfection and CS induction. Results showed that compared to si-NC, the average fluorescence intensity of MitoSOX was significantly higher in the si-CISD1 group (Fig. 2E). Similarly, compared to the si-NC group, the average fluorescence intensity of DCF was higher in the si-CISD1 group (Fig. 2F).

Moreover, compared to the NC group, the average fluorescence intensity of MitoSOX was higher in the 2%CSE group, suggesting higher mitochondrial ROS

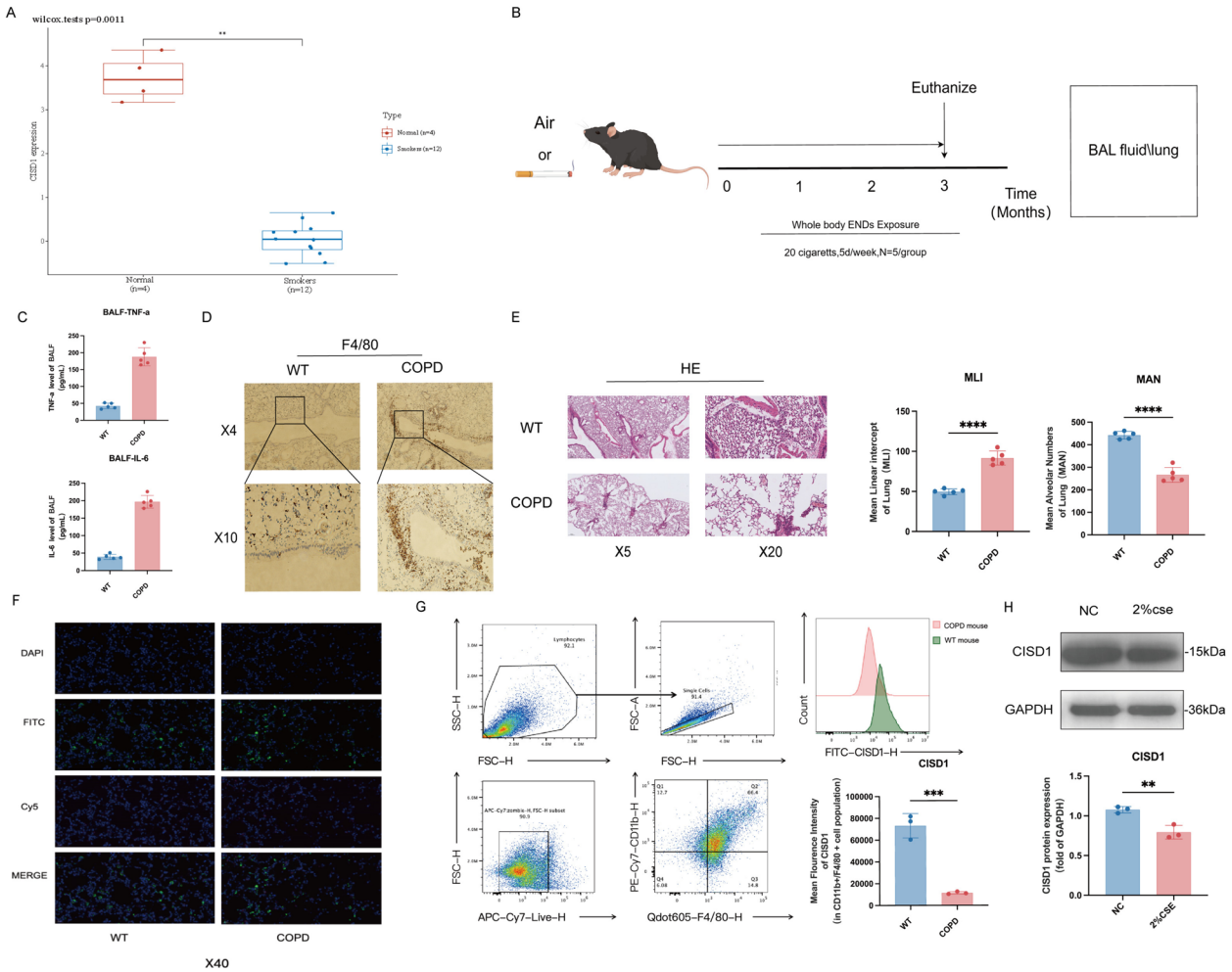

Fig. 1 Smoke exposure leads to a decrease in CISD1 expression in monocyte-derived macrophages. **A** Analysis of CISD1 expression levels in peripheral blood mononuclear cells of two groups (normal individuals and smokers) using a biological information database. **B** Exposure to cigarette smoke for 3 months to obtain a COPD mouse model. **C** Levels of TNF-a and IL-6 in BALF. **D** Localization of macrophages in lung tissue labeled with F4/80. **E** HE staining of lung tissue. **F** Immunofluorescence co-localization results of macrophages and CISD1. **G** Detection of CISD1 expression in monocytes from mouse lung tissue using flow cytometry. **H** Detection of CISD1 protein expression levels using Western Blot after 24 h of stimulation with 2% cigarette smoke extract (2% CSE) in Raw264.7 cells. Values represent mean ± SD, n = 5 for each group. *p < 0.05, **p < 0.01, ***p < 0.001,****p < 0.0001

levels (Fig. 2H). Similarly, compared to the NC group, the average fluorescence intensity of DCF was higher in the 2%CSE group, indicating increased cellular oxidative stress and ROS production (Fig. 2I). The figures also display the JC-1 levels for the NC and 2%CSE groups, as well as the si-NC and si-CISD1 groups. The ratio of aggregates/monomers (red/green) in the NC and 2%CSE groups was 7.35 and 2.88, respectively, with lower values indicating fewer healthy mitochondria and greater mitochondrial damage. For the si-NC and si-CISD1 groups, the ratio of aggregates/monomers (red/green) was 19.8 and 8.75, respectively (Fig. 2G).

Inhibition of CISD1 activates the autophagy pathway in Raw264.7 cells

We conducted sequencing analysis on Raw264.7 cells after si-CISD1 transfection and found that compared to the si-NC group, a total of 29,424 genes were identified (Fig. 3A). In addition, we displayed a heatmap of the top 20 genes with significant differences (Fig. 3B). Based on log standard padj < 0.05 and |log2FC| ≥ 2 criteria, we identified 7,595 downregulated genes and 399 upregulated genes (Fig. 3C). Subsequent enrichment analysis revealed that CISD1 was associated with biological activities such as olfactory receptor activity, sensory perception of smell, odorant binding, Maturity onset

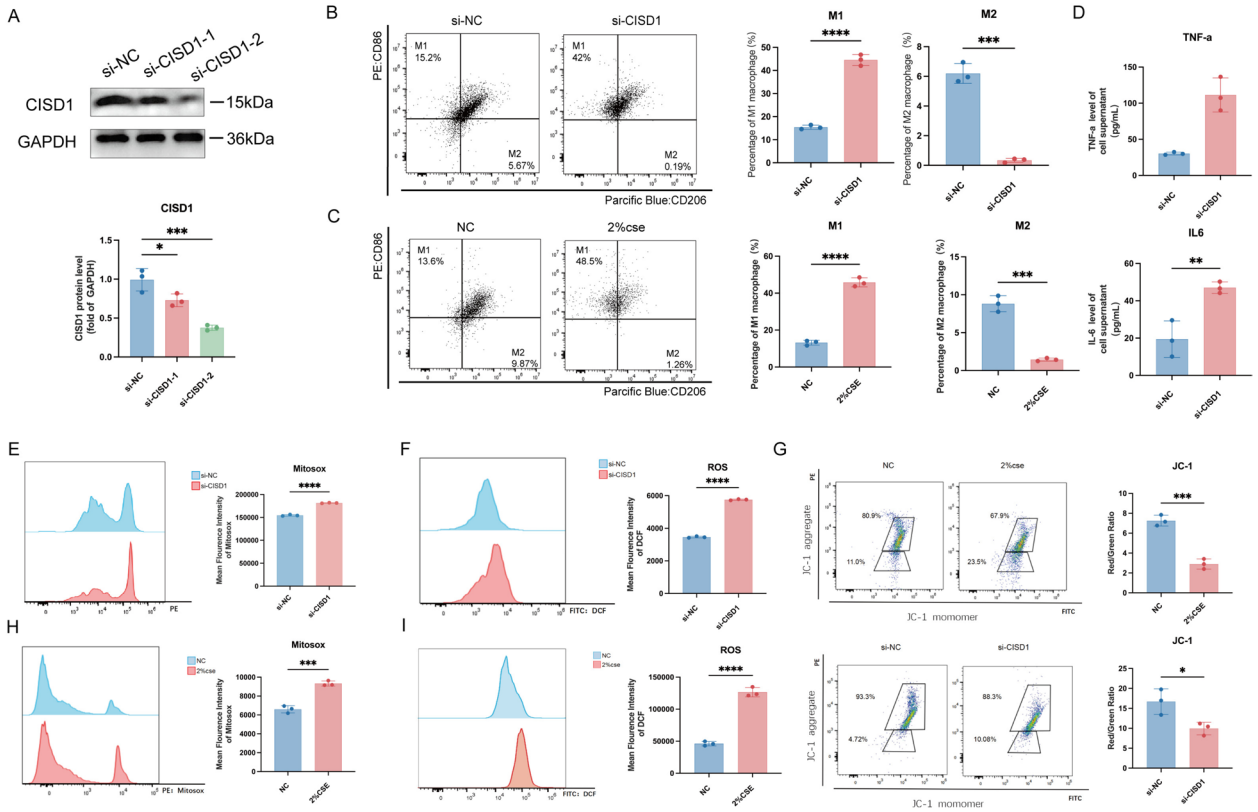

Fig. 2 Inhibiting CISD1 expression promotes macrophage polarization towards the M1 phenotype and inhibits M2 phenotype polarization. **A** Screening of si-CISD1 sequences, followed by Western Blot to detect CISD1 protein expression levels. **B** Detection of M1/M2 polarization using flow cytometry after si-CISD1 transfection into Raw264.7 cells for 24 h. **C** Detection of M1/M2 polarization using flow cytometry after stimulation of Raw264.7 cells with 2% cigarette smoke extract (2% CSE) for 24 h. **D** Levels of IL-6 and TNF-a inflammatory factors in the cell supernatant after si-CISD1 transfection. **E**, **F** Measurement of Mitosox fluorescence intensity (mitochondrial ROS levels) and DCFH-DA fluorescence intensity (cellular ROS levels) after si-CISD1 transfection. **H**, **I** Measurement of mitochondrial ROS levels and cellular ROS levels after stimulation of Raw264.7 cells with 2% CSE for 24 h. **G** Evaluation of mitochondrial membrane potential damage under different treatments by measuring JC-1 levels after stimulation of Raw264.7 cells with 2% CSE and si-CISD1, respectively, for a certain period of time. Values represent mean ± SD, n = 3 for each group. *p < 0.05, **p < 0.01, ***p < 0.001, ****p < 0.0001

diabetes of the young, and Nicotine addiction (Fig. 3D, E). More importantly, through GSEA enrichment analysis, we found a significant correlation between CISD1 and the autophagy pathway (Fig. 3F). Finally, Western blotting results verified that compared to the si-NC group, the si-CISD1 group exhibited higher expression of LC3A/B protein, lower levels of SQSTM1/p62 protein, and increased levels of mitochondrial autophagy-related proteins PINK1 and PARKN (Fig. 3G). This indicates that inhibition of CISD1 expression significantly activates the autophagy pathway in Raw264.7 cells and enhances Parkin-dependent mitochondrial autophagy activity.

(See figure on next page.)

Fig. 3 Inhibition of CISD1 activates the autophagy pathway in Raw264.7 cells. **A** Differential genes identified from high-throughput sequencing results after si-CISD1 treatment. **B** Heatmap showing the expression levels of 20 differential genes. **C** Upregulated and downregulated genes enriched under selected criteria. **D** Gene ontology (GO) functional enrichment analysis. **E** Kyoto encyclopedia of genes and genomes (KEGG) pathway enrichment analysis. **F** Gene set enrichment analysis (GSEA) enrichment in the autophagy pathway. **G** Detection of CISD1、some mitophagy LC3A/B、PINK1、PARKN、SQSTM1/p62 protein expression levels using Western Blot after 24 h of stimulation with si-CISD1/si-NC entered in Raw264.7 cells. Values represent mean ± SD, n = 3 for each group. *p < 0.05, **p < 0.01, ***p < 0.001, ****p < 0.0001

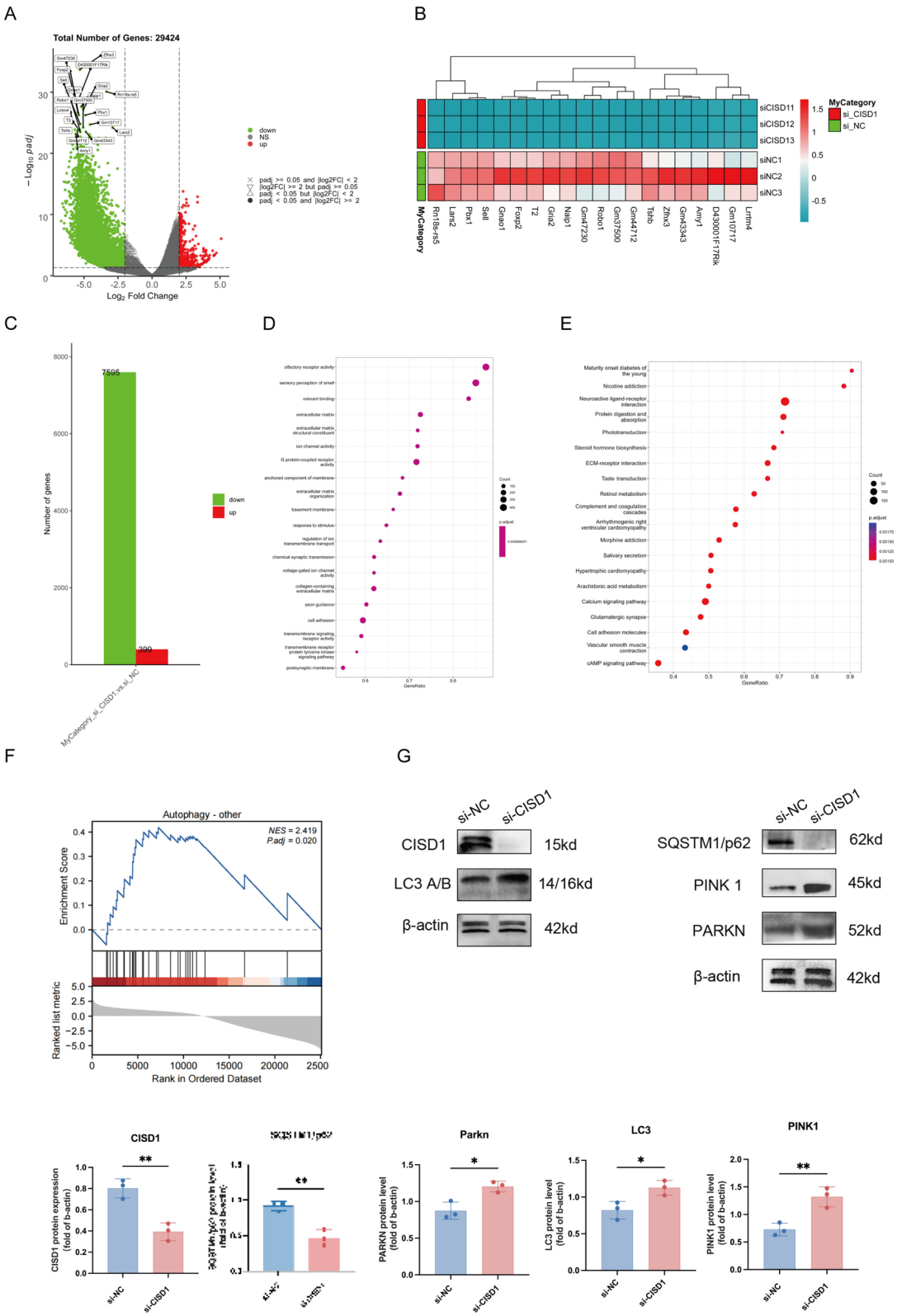

Fig. 3 (See legend on previous page.)

Inhibition of autophagy leads to an increase in M2 polarization and a decrease in M1 polarization in Raw264.7 cells, accompanied by significant restoration of mitochondrial function and reduction in oxidative stress levels

To further investigate the relationship between CISD1 and autophagy, we introduced the autophagy inhibitor 3-MA. After inhibiting autophagy, in the DMSO group, compared to si-NC, transfection with si-CISD1 resulted in increased cellular ROS generation. Both groups with the addition of the 3-MA inhibitor showed a decrease in ROS generation compared to the DMSO group. In the 3-MA group, cells transfected with si-CISD1 showed higher ROS levels than the si-NC group. There were statistically significant differences in ROS levels among the four groups (Fig. 4A).

In the DMSO group, compared to si-NC, transfection with si-CISD1 resulted in an increase in M1 macrophage polarization from 22.1% to 25.2% and a decrease in M2 polarization from 14.5% to 11.4%. Comparing to the DMSO group, both M1 and M2 polarization increased in the groups with the addition of 3-MA inhibitor, with M1 macrophages increasing from 14.5% to 57.5%. Furthermore, in the 3-MA group, transfection with si-CISD1 led to higher levels of M1 macrophage polarization compared to the si-NC group, at 8.53% and 1.54%, respectively, while M2 macrophage polarization was lower at 32.9% compared to 57.5% in the si-NC group. There were statistically significant differences in the polarization degrees of M1 and M2 macrophages among the four groups, as well as in the M1/M2 ratio (Fig. 4B, C).

We also observed that mitochondrial ROS production levels, as indicated by Mitosox, were higher in

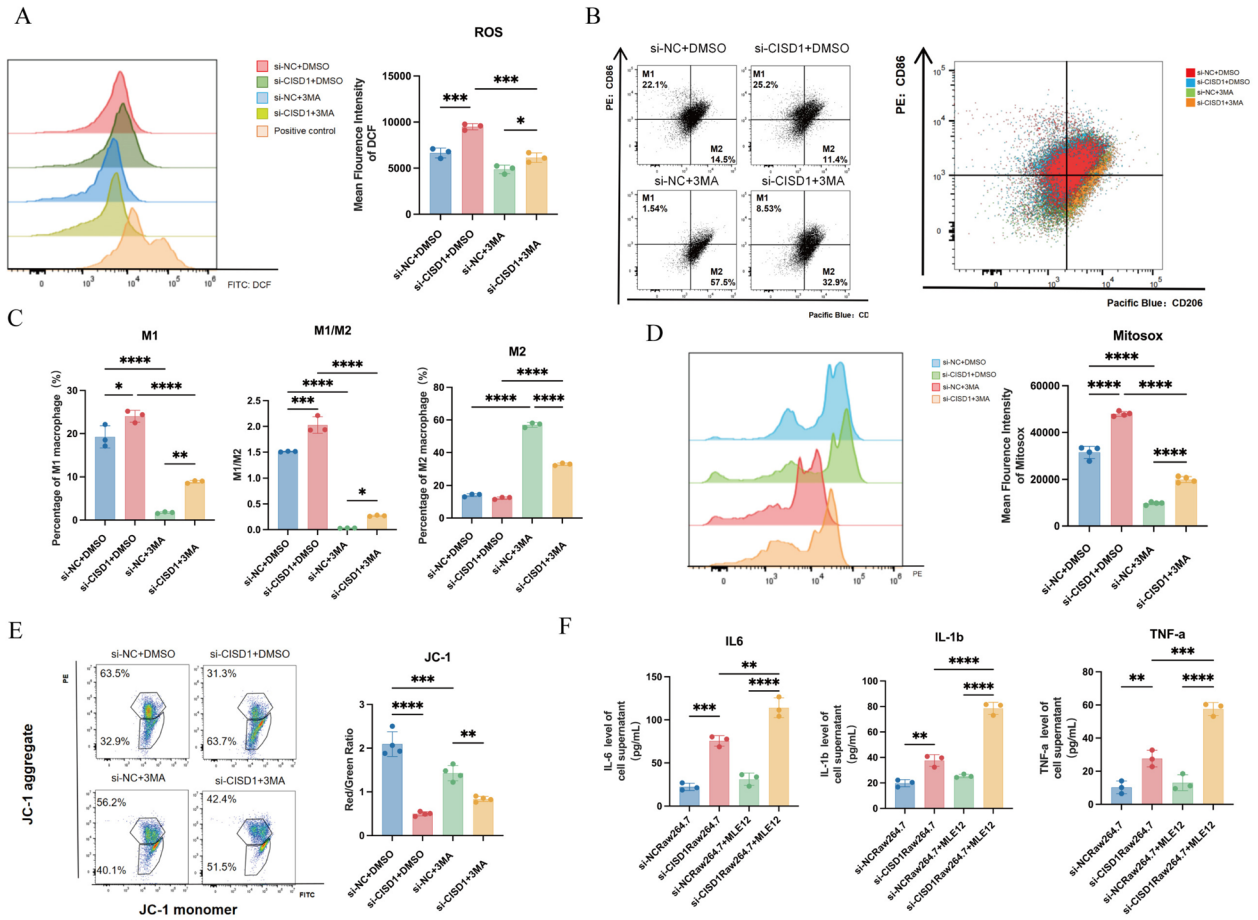

Fig. 4 Inhibition of autophagy leads to an increase in M2 polarization and a decrease in M1 polarization in Raw264.7 cells, accompanied by significant restoration of mitochondrial function and reduction in oxidative stress levels. **A** In addition to the addition of si-CISD1, the autophagy inhibitor 3-MA was added to detect cellular ROS levels. **B** Detection of M1/M2 polarization of Raw264.7 cells. **C** Statistical demonstration of M1/M2 polarization of Raw264.7 cells. **D** Detection of mitosox fluorescence intensity. **E** Detection of JC-1 levels. **F** Co-culture of Raw264.7 and MLE12 (Raw 264.7 was treated with si-CISD1 and si-NC) to detect IL-1b, TNF-a, IL-6 levels. Values represent mean ± SD, n = 3 for each group. *p < 0.05, **p < 0.01, ***p < 0.001,****p < 0.0001

the si-CISD1 group compared to si-NC, indicating an increase in mitochondrial ROS production. In addition, in the 3-MA group, while overall immunofluorescence intensity decreased, the average fluorescence intensity of si-CISD1 remained higher than si-NC, suggesting a decrease in mitochondrial ROS levels after autophagy inhibition, but the levels remained higher in the si-CISD1 group compared to the control group (Fig. 4D).

Furthermore, we examined the JC-1 index of the four groups, indicating the degree of mitochondrial membrane potential (MMP). In the DMSO group, the Red/Green ratio in the si-CISD1 group was lower compared to si-NC, indicating a decrease in MMP and greater mitochondrial damage. After adding the 3-MA inhibitor, the si-NC group showed fewer healthy mitochondria in macrophages compared to the si-NC + DMSO group, while the si-CISD1 + 3MA group exhibited greater mitochondrial damage in macrophages compared to the si-DMSO group. There were statistically significant differences in mitochondrial membrane potential (MMP) among the four groups (Fig. 4E).

Next, we investigated whether si-CISD1 in Raw264.7 cells affected the production of more inflammatory factors by MLE12 cells, leading to COPD inflammation. The results showed that after co-culturing with MLE12 cells, the levels of inflammatory molecules IL-6, TNF-α, and IL-1β in the supernatant were elevated in the si-CISD1Raw264.7 group compared to si-NC, suggesting that the production of inflammatory factors or changes in the microenvironment induced by si-CISD1Raw264.7 promoted the production of inflammatory factors by MLE12 cells (Fig. 4F).

Combining the expression of autophagy pathway proteins, we hypothesize that inhibition of CISD1 may promote M1 macrophage polarization by activating the autophagy pathway, leading to the aforementioned changes in mitochondrial phenotypes.

Discussion

CISD1 is a member of the NEET protein family, characterized by its close association with cell death, ferroptosis, cellular ROS regulation, and mitochondrial dysfunction [20, 21]. Some studies suggest that CISD1 is detrimental in the context of ferroptosis, as its inhibition can alleviate GSH-induced iron-dependent cell death in myocardial cells [22]. In recent years, the role of CISD1 in mitochondrial function has been increasingly highlighted. Research on certain neurodegenerative diseases suggests that mitochondrial dysfunction is a key pathogenic mechanism of Parkinson's disease (PD) [23]. CISD1 can directly interact with Parkin, promoting the ubiquitination of mitochondrial proteins, thereby playing a crucial role in mitochondrial quality control [24, 25].

In some lung diseases, epithelial cells are the primary cell type involved; however, the role of immune cells cannot be overlooked. Numerous studies have demonstrated that macrophages play a significant role in the development of COPD [26, 27]. Smoking has been shown to disrupt ROS balance in macrophages [28]. Studies on asthma have indicated increased infiltration of M2-type macrophages in asthma patients compared to healthy controls [29]. Interestingly, in our study, following the stimulation of Raw264.7 cells with smoke, there was a notable increase in M1-type macrophages. Moreover, transfection with si-CISD1 led to an increase in M1-type macrophages and a reduction in M2-type macrophages.

CISD1 has been studied in asthma and acute lung injury. Compared to healthy or untreated groups, CISD1 expression is upregulated in epithelial cells in asthma groups [29]. A similar upregulation of CISD1 has been observed in epithelial cells during acute lung injury [30]. In contrast, in cardiovascular diseases, CISD1 expression is significantly reduced in lipid-rich THP1 macrophages [10]. Consistently, in this study, CISD1 expression decreased after smoke stimulation of Raw264.7 cells. Therefore, we suggest that the reduction in CISD1 levels in macrophages may be linked to the immune microenvironment and may play a role in regulating it. This regulation could potentially impact various physiological activities of macrophages, such as ROS homeostasis, maintenance of mitochondrial membrane potential (MMP), and macrophage phenotype modulation.

Mechanistically, the reversal of mitochondrial dysfunction by CISD1 may occur through certain pathways. However, there are not many studies on these pathways. Most studies have revealed the interaction of CISD1 with certain proteins. For example, some studies have found that CISD1 can interact with dynamin-related protein 1 (Drp1) [10]. In this experiment, mitochondrial dysfunction and the extent of M1 polarization in si-CISD1-treated Raw264.7 cells were mitigated by the autophagy inhibitor 3-MA [31]. Another study suggests that CISD1 plays a critical role in autophagy regulation. It was found that CISD1 overexpression effectively inhibited autophagic cell death and physiological dysfunction in the brains of neonates with hypoxic–ischemic injury [32]. Moreover, this study also observed that CISD1 overexpression is associated with the reversal of mitochondrial dysfunction in macrophages, while si-CISD1 transfection exacerbates the adverse mitochondrial dysfunction phenotype in macrophages. The relationship between CISD1 and autophagy is also evident at the protein level [33]. After si-CISD1 transfection, autophagy-related proteins, such as LC3 and p62, were upregulated in macrophages, indicating a close association between CISD1 and autophagy activation [34]. CISD1 may also

activate mitochondrial autophagy to some extent. The Parkin E3 ligase activity of CISD1 has been shown to enhance AMPK activation, thereby promoting mitochondrial autophagy in a PINK1–Parkin-independent manner [35–37]. These findings suggest that CISD1 plays an essential role in activating autophagy and mitochondrial autophagy pathways, as demonstrated by our study. In addition, some studies have found that inhibition of CISD1 expression in Raw264.7 cells via NL-1 or si-CISD1 transfection induces PINK1/Parkin-mediated mitochondrial autophagy [38]. This finding is partly consistent with the results of our study. Furthermore, we explored the relationship between CISD1 and M1/M2 macrophages and found that CISD1 inhibition may affect M1/M2 polarization through autophagy activation. Upon autophagy inhibition, there was an increase in M2 polarization and a decrease in M1 polarization in macrophages.

The interaction between pulmonary epithelial cells and macrophages plays a crucial role in the development and pathophysiology of COPD [39]. Macrophages are influenced by inflammatory cytokines such as interleukin-1β (IL-1β) and tumor necrosis factor-α (TNF-α), which regulate the inflammatory and immune responses of pulmonary epithelial cells, thereby influencing disease progression [40]. Tobacco smoke and other harmful gases induce oxidative stress, increasing the production of oxidants [41]. Macrophages contribute to oxidative stress by releasing reactive oxygen species and other oxidants, which can impair the function and survival of pulmonary epithelial cells [42]. COPD results in an imbalance in the repair processes of damaged pulmonary epithelial cells, with macrophages playing a significant role by releasing pro-inflammatory cytokines and growth factors that affect epithelial proliferation and repair. However, in COPD, these repair processes are often incomplete, contributing to further declines in lung function [43]. Both pulmonary epithelial cells and macrophages are involved in regulating pulmonary immune responses. In COPD, chronic inflammation impairs immune regulatory functions, leading to immune imbalance and increased susceptibility to infections, making COPD patients more prone to respiratory infections [44].

The relationship between macrophages and epithelial cells in COPD has been relatively understudied. To address this, our study co-cultured Raw 264.7 macrophages with MLE12 epithelial cells. The results showed that, following CISD1 transfection into Raw 264.7 cells, MLE12 cells produced classical inflammatory factors such as TNF-α, IL-6, and IL-1β. These findings suggest that COPD progression is facilitated by multicellular-mediated inflammation. In addition, we speculate that the inflammatory factors produced by si-CISD1-treated Raw 264.7 cells promote inflammatory responses in epithelial cells, thereby illustrating how immune microenvironment cells can generate harmful stimuli to epithelial cells and further exacerbate the inflammatory response.

The reversal of LPS-induced inflammatory effects by inhibiting CISD1 has been explored in related studies [45], and these results appear consistent with our findings. However, it is important to note that this perspective is based on subsequent studies involving CISD1 upregulation in epithelial cells, which differs from the current investigation into the role of CISD1 in macrophages. This paper also discusses how changes in CISD1 expression in macrophages affect epithelial cells, focusing primarily on the impact of CISD1 on the immune microenvironment.

Although this study did not identify the specific substances produced by M1 macrophages after CISD1 inhibition that directly lead to epithelial cell responses, we believe our research holds substantial value. It provides a preliminary understanding of the role CISD1 may play in the interaction between macrophages and epithelial cells in COPD pathogenesis, paving the way for further investigation into the mechanistic role of CISD1 in COPD. Moreover, this research may offer potential immunotherapeutic targets for the clinical treatment of COPD. Increasing CISD1 expression could potentially serve as a novel therapeutic strategy for managing COPD [46].

Conclusion

Smoke exposure can suppress CISD1 expression in macrophages, which may contribute to M1 polarization, mitochondrial dysfunction, and cellular oxidative stress imbalance, potentially linked to the activation of the autophagy pathway. In addition, we observed that CISD1 knockdown in macrophages might promote the production of inflammatory factors in epithelial cells, collectively contributing to COPD pathogenesis. While this study provides valuable insights into the role of CISD1 in COPD, there are several limitations. First, the use of cell lines and mouse models, though informative, may not fully capture the complexity of human COPD. Using patient-derived macrophages or primary human cells could provide more clinically relevant data. In future studies, we plan to incorporate clinical samples to better evaluate the function and mechanisms of CISD1 in human COPD, with the aim of improving our understanding of its role in disease progression. In addition, although we observed CISD1's involvement in mitochondrial dysfunction and M1 polarization, the precise molecular mechanisms underlying these processes remain unclear. The current study lacks detailed analysis of the signaling pathways and downstream mediators

that could explain how CISD1 modulates these effects, necessitating further investigation.

Supplementary Information

The online version contains supplementary material available at https://doi.org/10.1186/s40001-024-02146-2.

Additional file 1

Acknowledgements
Not applicable.

Author contributions
This study was equally contributed by Jiameng Gao, Meiyuan Dong and Weibin Tian. Study concept and design: Jiameng Gao and Meiyuan Dong. Jiameng Gao, Zhilong Jiang,Weibin Tian, Meiyuan Dong and Junyi Xia conducted experiments and collected data. Data interpretation and statistical analysis: Jiameng Gao, Weibin Tian and Yuhao Qian. The manuscript was drafted by Jiameng Gao. Study supervision:Yao Shen and Zhihong Chen.

Funding
The present study was supported by the Natural Science Foundation of Shanghai (grant no.20Z11901004, 20Z11901000), Shanghai Pudong Hospital and the Discipline Construction Promoting Project of Shanghai Pudong Hospital (grant no. Zdzk2020-11).

Availability of data and materials
No datasets were generated or analysed during the current study.

Declarations

Ethics approval and consent to participate
The study was conducted under the approval of the Ethics Committee of Shanghai Pudong Hospital (SKWXZ-01). All animal experiment procedures were conducted per the Guide for the Care and Use of Laboratory Animals.

Consent for publication
Not applicable.

Competing interests
The authors declare no competing interests.

Author details
[1]Department of Respiratory and Critical Care Medicine, Shanghai Pudong Hospital, 2800 Gongwei Rd, Shanghai 201399, China. [2]Department of Respiratory and Critical Care Medicine of Zhongshan Hospital, Shanghai Institute of Respiratory Disease, Fudan University, Shanghai, People's Republic of China.

Received: 26 June 2024 Accepted: 5 November 2024
Published online: 13 November 2024

References

1. Ashrafi G, Schwarz TL. The pathways of mitophagy for quality control and clearance of mitochondria. Cell Death Differ. 2013;20(1):31–42.
2. Barnes PJ. Oxidative stress-based therapeutics in COPD. Redox Biol. 2020;33: 101544.
3. Bissonnette EY, Lauzon-Joset JF, Debley JS, et al. Cross-talk between alveolar macrophages and lung epithelial cells is essential to maintain lung homeostasis. Front Immunol. 2020;11: 583042.
4. Bravo-San Pedro JM, Kroemer G, Galluzzi L. Autophagy and mitophagy in cardiovascular disease. Circ Res. 2017;120(11):1812–24.
5. Caramori G, Casolari P, Barczyk A, et al. COPD immunopathology. Semin Immunopathol. 2016;38(4):497–515.
6. Christenson SA, Smith BM, Bafadhel M, et al. Chronic obstructive pulmonary disease. Lancet. 2022;399(10342):2227–42.
7. Geldenhuys WJ, Benkovic SA, Lin L, et al. MitoNEET (CISD1) knockout mice show signs of striatal mitochondrial dysfunction and a Parkinson's disease phenotype. ACS Chem Neurosci. 2017;8(12):2759–65.
8. Goh F, Shaw JG, Savarimuthu Francis SM, et al. Personalizing and targeting therapy for COPD: the role of molecular and clinical biomarkers. Expert Rev Respir Med. 2013;7(6):593–605.
9. Halpin DMG, Criner GJ, Papi A, et al. Global initiative for the diagnosis, management, and prevention of chronic obstructive lung disease the 2020 gold science committee report on COVID-19 and chronic obstructive pulmonary disease. Am J Respir Crit Care Med. 2021;203(1):24–36.
10. Ham SJ, Yoo H, Woo D, et al. PINK1 and Parkin regulate IP(3)R-mediated ER calcium release. Nat Commun. 2023;14(1):5202.
11. Han R, Liu Y, Li S, et al. PINK1-PRKN mediated mitophagy: differences between in vitro and in vivo models. Autophagy. 2023;19(5):1396–405.
12. He BF, Wu YX, Hu WP, et al. ROS induced the Rab26 promoter hypermethylation to promote cigarette smoking-induced airway epithelial inflammation of COPD through activation of MAPK signaling. Free Radic Biol Med. 2023;195:359–70.
13 Barrett T, Wilhite SE, Ledoux P, et al. NCBI GEO: archive for functional genomics data sets–update. Nucleic Acids Res. 2013;41:991–5.
14. Sun J, Huang J, Lan J, et al. Overexpression of CENPF correlates with poor prognosis and tumor bone metastasis in breast cancer. Cancer Cell Int. 2019;19:264.
15. Zhang X, Zhang W, Jiang Y, et al. Identification of functional lncRNAs in gastric cancer by integrative analysis of GEO and TCGA data. J Cell Biochem. 2019;120(10):17898–911.
16. Zhang W, Zhang Y, Zhu Q. Cigarette smoke extract-mediated FABP4 upregulation suppresses viability and induces apoptosis, inflammation and oxidative stress of bronchial epithelial cells by activating p38 MAPK/MK2 Signaling pathway. J Inflamm. 2022;19(1):7.
17. Hua J, Gao Z, Zhong S, et al. CISD1 protects against atherosclerosis by suppressing lipid accumulation and inflammation via mediating Drp1. Biochem Biophys Res Commun. 2021;577:80–8.
18 Cipollina C, Bruno A, Fasola S, et al. Cellular and molecular signatures of oxidative stress in bronchial epithelial cell models injured by cigarette smoke extract. Int J Mol Sci. 2022. https://doi.org/10.3390/ijms23031770.
19. Xia D, Liu J, Yong J, et al. Strategies for understanding the role of cellular heterogeneity in the pathogenesis of lung cancer: a cell model for chronic exposure to cigarette smoke extract. BMC Pulm Med. 2022;22(1):333.
20. Larson-Casey JL, He C, Carter AB. Mitochondrial quality control in pulmonary fibrosis. Redox Biol. 2020;33: 101426.
21 Lee JW, Chun W, Lee HJ, et al. The role of macrophages in the development of acute and chronic inflammatory lung diseases. Cells. 2021. https://doi.org/10.3390/cells10040897.
22. Lee S, Lee S, Lee SJ, et al. Inhibition of mitoNEET induces Pink1-Parkin-mediated mitophagy. BMB Rep. 2022;55(7):354–9.
23. Lee S, Seok BG, Lee SJ, et al. Inhibition of mitoNEET attenuates LPS-induced inflammation and oxidative stress. Cell Death Dis. 2022;13(2):127.
24. Li FJ, Fu S, Ye H, et al. Metallothionein alleviates glutathione depletion-induced oxidative cardiomyopathy through CISD1-dependent regulation of ferroptosis in murine hearts. Am J Pathol. 2024;194(6):912–26.
25. Lipper CH, Stofleth JT, Bai F, et al. Redox-dependent gating of VDAC by mitoNEET. Proc Natl Acad Sci U S A. 2019;116(40):19924–9.
26 Liu F, Dong Y, Zhong F, et al. CISD1 is a breast cancer prognostic biomarker associated with diabetes mellitus. Biomolecules. 2022. https://doi.org/10.3390/biom13010037.
27 Palikaras K, Lionaki E, Tavernarakis N. Coordination of mitophagy and mitochondrial biogenesis during ageing in C elegans. Nature. 2015;521(7553):525–8.
28. Paplinska-Goryca M, Misiukiewicz-Stepien P, Nejman-Gryz P, et al. Epithelial-macrophage-dendritic cell interactions impact alarmins expression in asthma and COPD. Clin Immunol. 2020;215: 108421.
29. Pickrell AM, Youle RJ. The roles of PINK1, parkin, and mitochondrial fidelity in Parkinson's disease. Neuron. 2015;85(2):257–73.
30. Ploumi C, Kyriakakis E, Tavernarakis N. Coupling of autophagy and the mitochondrial intrinsic apoptosis pathway modulates proteostasis and ageing in Caenorhabditis elegans. Cell Death Dis. 2023;14(2):110.
31. Racanelli AC, Kikkers SA, Choi AMK, et al. Autophagy and inflammation in chronic respiratory disease. Autophagy. 2018;14(2):221–32.

32. Seabright AP, Fine NHF, Barlow JP, et al. AMPK activation induces mitophagy and promotes mitochondrial fission while activating TBK1 in a PINK1-Parkin independent manner. Faseb J. 2020;34(5):6284–301.
33. Shapouri-Moghaddam A, Mohammadian S, Vazini H, et al. Macrophage plasticity, polarization, and function in health and disease. J Cell Physiol. 2018;233(9):6425–40.
34. Shi Y, Tao M, Ma X, et al. Delayed treatment with an autophagy inhibitor 3-MA alleviates the progression of hyperuricemic nephropathy. Cell Death Dis. 2020;11(6):467.
35. Sorrentino V, Menzies KJ, Auwerx J. Repairing mitochondrial dysfunction in disease. Annu Rev Pharmacol Toxicol. 2018;58:353–89.
36. Sun X, Liu Y, Feng X, et al. The key role of macrophage depolarization in the treatment of COPD with ergosterol both in vitro and in vivo. Int Immunopharmacol. 2020;79: 106086.
37. Trivedi A, Bade G, Madan K, et al. Effect of smoking and its cessation on the transcript profile of peripheral monocytes in COPD patients. Int J Chron Obstruct Pulmon Dis. 2022;17:65–77.
38. Upadhyay P, Wu CW, Pham A, et al. Animal models and mechanisms of tobacco smoke-induced chronic obstructive pulmonary disease (COPD). J Toxicol Environ Health B Crit Rev. 2023;26(5):275–305.
39. Wang H, Jia Y, Gu J, et al. Ferroptosis-related genes are involved in asthma and regulate the immune microenvironment. Front Pharmacol. 2023;14:1087557.
40. Wu MN, Zhou DM, Jiang CY, et al. Genetic analysis of potential biomarkers and therapeutic targets in ferroptosis from psoriasis. Front Immunol. 2022;13:1104462.
41 Yamasaki K, Eeden SFV. Lung macrophage phenotypes and functional responses: role in the pathogenesis of COPD. Int J Mol Sci. 2018. https://doi.org/10.3390/ijms19020582.
42. Yin K, Lee J, Liu Z, et al. Mitophagy protein PINK1 suppresses colon tumor growth by metabolic reprogramming via p53 activation and reducing acetyl-CoA production. Cell Death Differ. 2021;28(8):2421–35.
43. Zhang X, Peng T, Li C, et al. Inhibition of CISD1 alleviates mitochondrial dysfunction and ferroptosis in mice with acute lung injury. Int Immunopharmacol. 2024;130: 111685.
44. Zhang ZB, Xiong LL, Xue LL, et al. MiR-127-3p targeting CISD1 regulates autophagy in hypoxic-ischemic cortex. Cell Death Dis. 2021;12(3):279.
45. Zhong G, Li Y, Li L, et al. Mitochondrial miR-12294-5p regulated copper-induced mitochondrial oxidative stress and mitochondrial quality control imbalance by targeted inhibition of CISD1 in chicken livers. J Hazard Mater. 2023;458: 131908.
46. Zi Y, Wang X, Zi Y, et al. Cigarette smoke induces the ROS accumulation and iNOS activation through deactivation of Nrf-2/SIRT3 axis to mediate the human bronchial epithelium ferroptosis. Free Radic Biol Med. 2023;200:73–86.

Publisher's Note